Published in final edited form as:

FASEB J. 2020 May ; 34(5): 6757–6768. doi:10.1096/fj.201903234R.

Yap1 is required for maintenance of adult RPE differentiation

Qingxian Lu, **Patrick A. Scott**, **Eric V. Vukmanic**, **Henry J. Kaplan**, **Douglas C. Dean**, **Qiutang Li**[1]

Departments of Ophthalmology and Visual Sciences, University of Louisville School of Medicine, Louisville, KY 40202, USA.

Abstract

Nuclear YAP1 plays a critical role in regulation of stem cell proliferation, tissue regeneration, and organ size in many types of epithelia. Due to rapid turnover of most epithelial cell types, the cytoplasmic function of YAP1 in epithelial cells has not been well studied. The retinal pigment epithelium (RPE) is a highly polarized epithelial cell type maintained at a senescence state, and offers an ideal cell model to study the active role of YAP1 in maintenance of the adult epithelial phenotype. Here we show that the cytoplasmic function of YAP1 is essential to maintain adult RPE differentiation. Knockout of *Yap1* in the adult mouse RPE caused cell depolarization and tight junction breakdown, and led to inhibition of RPE65 expression, diminishment of RPE pigments, and retraction of microvilli and basal infoldings. These changes in RPE further prompted the loss of adjacent photoreceptor outer segments and photoreceptor death, which eventually led to decline of visual function in older mice between 6–12 months of age. Furthermore, nuclear β-catenin and its activity were significantly increased in mutant RPE. These results suggest that YAP1 plays an important role in active inhibition of Wnt/β-catenin signaling, and is essential for downregulation of β-catenin nuclear activity and prevention of dedifferentiation of adult RPE.

Keywords

eye; dedifferentiation; EMT; Wnt/beta-catenin; RPE65; knockout

Introduction

During development, the transcription coactivator YAP1 is crucial in maintaining proliferation and dedifferentiation of progenitors, as organ and tissue fields are formed (1–4). As cells expand to fill developing fields, their cell-cell contacts trigger activation of the Hippo kinase cascade, which causes cytoplasmic retention of YAP1. This cytoplasmic retention persists in adult epithelial cells that are arrested by cell-cell contact. But, YAP1 translocates to the nucleus in epithelial basal progenitor cells as they proliferate for replacement of the mature epithelium. The Hippo pathway was initially identified for its

[1]Correspondence: Departments of Ophthalmology and Visual Sciences, University of Louisville, 301 East Muhammad Ali Blvd., Louisville, KY 40202, USA. q.li@louisville.edu.

Author Contributions

Q. Li and Q. Lu designed research; Q. Li, Q. Lu, Scott, H., D. Dean, and Kaplan analyzed data; Q. Lu, Q. Li P. Scott, E. Vukmanic performed research; Q. Li, Q. Lu, P. Scott, D. Dean, and H. Kaplan wrote the paper.

function in regulating cell proliferation and cell death in flies, and is a well-conserved pathway in mammals. YAP1 is a major transcriptional effector of the evolutionary conserved Hippo pathway in mammals, and it shuttles between the cytoplasm and nucleus through the regulation of the Hippo kinase cascade. Activation of Hippo pathway leads to phosphorylation and inactivation of YAP1 by cytoplasmic retention (2, 3). YAP1 lacks a DNA binding domain and its nuclear function depends upon heterodimerization with other DNA binding transcription factors, including Tead1, Smads, and β-catenin (3–7). YAP1 is retained in the cytoplasm through interaction with α-catenin, angiomotin and disheveled (DVL) (6, 8–17). Adherens junction-related α-catenins and the tight junction -associated proteins, angiomotin and angiomotin-like 1/2, can directly interact with YAP1 and sequester it in the cytoplasm, thus modulating the level of YAP1 phosphorylation and its activity. Changes in cell contact and loss of α-catenin and AMOT family proteins cause YAP1 nuclear activation and cell transformation (14). DVL is a scaffolding protein moving between the cytoplasm and nucleus, and an important regulator for Wnt/β-catenin signaling. It has been shown that DVL is responsible for cytosolic translocation of phosphorylated YAP (18). Inactivating mutation of the nuclear export signal embedded in DVL leads to nuclear YAP retention, with an increase in TEAD transcriptional activity (18).

It has been presumed that this cytoplasmic retention simply prevents nuclear translocation of YAP1 thereby causing its inactivation. However, it is also possible that retention of YAP1 in the cytoplasm is serving to prevent nuclear translocation, and thus, the activity of transcription factors that complex with YAP1 in the cytoplasm. For example, is there a role for YAP1 in the cytoplasm of mature epithelial cells in sequestering transcription factors such as β-catenin to effectively prevent Wnt signaling in the adult cells? Experiments evaluating the role of Yap1 in epithelium are complicated by the rapid turnover of epithelium examined to date and it is difficult to dissect or separate Yap1 function in basal cell mediated repopulation of epithelium from a possible role in the cytoplasm of adult cells. The RPE serves as a blood outer retinal barrier critical for adjacent photoreceptor function in the retina (19). In contrast to other epithelial cells, the RPE is long-lived, and cell replacement is not detected *in vivo*, making this population ideal for evaluation of YAP function in adult epithelium.

Hippo signaling is critical for *Drosophila* eye development and zebrafish retinogenesis (4, 20–23). The nuclear YAP1 is present in early developing RPE cells, and important for progenitor proliferation and RPE specification in zebrafish (21). Similarly, RPE trans-differentiates into epithelium with retinal characteristics in *Yap1* conditional knockout (cKO) mice during ocular development (24). RPE proliferation stops during RPE differentiation and maturation process at postnatal day 7–10 (25, 26). It is unclear whether the Yap1 has an active role in the post-mitotic adult RPE. Here we aim to dissect Yap1 function and its regulatory mechanism in the fully differentiated adult RPE by generating *Yap1* cKO specifically in differentiated RPE cells.

Material and Methods

Ethics statement

All animal experimental procedures were approved by Institutional Animal Care and Use Committee, the Animal Care Committee at the University of Louisville, and were conducted in accordance with the guidelines of Association for Research in Vision and Ophthalmology on the use of animals in research.

Mice and genotyping

Best1-Cre mice (stock # 017557) (27) and *ROSA26-flox-STOP-flox-GFP* mice (stock #007676) (28) were purchased from The Jackson Laboratory (Bar Harbor, ME, USA), and used to set up a breeding colony. *Yap1*$^{fl/fl}$ mice were purchased from NIH supported Mutant Mouse Resource & Research Center (MMRRC) at UC Davis (Davis, CA, USA). Experimental animals were housed under pathogen-free conditions and handled in accordance with guidelines approved by the Institutional Animal Care and Use Committee of the University of Louisville. Genotypes were determined by performing PCR amplification based on the information provided by vendors.

Mouse fundus examination

In vivo fundoscopy was conducted using a retinal camera (model TRC 50X; Topcon America Corp., Paramus, NJ, USA) with Canon 5D digital imaging hardware. To enhance the view of the small eye, a 2.2 Volk Panretinal lens (Volk Optical Inc., Mentor, OH, USA) was attached to the front of the lens on a clinical fundus camera. Fundus examination was performed by dilation with a single drop mixture of 0.06% tropicamide and 0.3% phenylephrine hydrochloride to dilate or enlarge the pupil for a better view of the fundus of the eye.

Electroretinography (ERG)

Topical applications of 2.5% phenylephrine hydrochloride and 1% tropicamide drops were administered to induce mydriasis of the pupils and to inhibit accommodation. Anesthesia was maintained with an intraperitoneal injection of the anesthetic ketamine (12.2 mg/mL) / xylazine (4.9 mg/mL) mixture solution at 0.05 mL per 10 g body weight.

The full field ERG (ffERG) was measured bilaterally using rodent ERG electrodes (LKC Technologies, Inc., Gaithersburg, MD, USA) placed on the cornea with methylcellulose (2%, Gonak; Akorn, Lake Forest, IL, USA) as described previously (29). A ground electrode was placed behind the ear and a reference electrode was on the midline of the forehead. The ffERG was recorded using a UTAS ERG system with a BigShot Ganzfeld (LKC Technologies, Inc., Gaithersburg, MD, USA). Mice were dark-adapted for 3 hours and the scotopic ERG was recorded first, using a strobe flash intensity of strobe flashes of 0.01, 0.03, and 0.3 cd/m^2. An averaged response was based on 15 presentations with a 2-second interstimulus interval. The animal was then light adapted with a 20 cd/m^2 background for 10 min and a series of ffERG responses were recorded at flash luminance of 1 and 3 cd/m^2. Measures of a- and b-waves were obtained from averaged responses to a single flash

intensity. The a-wave is defined as baseline to trough and the b-wave from a-wave trough to peak.

Histology and immunostaining

Mice were euthanized by CO_2 asphyxiation followed by cervical dislocation, and the enucleated eyes were immersion-fixed for overnight in 4% paraformaldehyde (PFA) in PBS, pH 7.4. In the following day, the eyes were subjected to OCT or paraffin embedding and sectioning for histological studies. The paraffin-embedded sections (7 μm thick) were prepared for hematoxylin and eosin (HE) staining. For most immunostaining, the tissue sections or cultured cell preparations were subjected to an antigen-retrieval procedure by heating the slides at 95°C for 30 min in 10 mM Tris-ethylendiaminetetraacetic acid (EDTA) buffer, pH 9.0. The primary antibodies used in this study were chicken anti-GFP (1:200, cat. #GFP-1020, Aves Lab, Inc., Tigard, OR, USA), and mouse anti-YAP1 (1:100, cat. # 56701, Abcam, Cambridge, MA, USA), mouse anti-YAP1 (1:100, cat. # sc-101199, Santa Cruz Biotechnology, Santa Cruz, CA, USA), rabbit anti-Ezrin (1;100, cat. # 3145S, Cell Signaling Technology, Danvers, MA, USA), mouse anti-RPE65 (1:100, cat. # MB5428, MilliporeSigma, Burlingto, MA, USA), TRITC anti-phalloidin (1:300, cat. # P1951, Sigma-Aldrich, St. Louis, MO, USA), mouse anti-β-catenin (1:100, cat. # BD 610154, BD Biosciences, Franklin Lakes, NJ, USA), rabbit anti-β-catenin (D10A8) (1;100, cat. # 8480S, Cell Signaling Technology, Danvers, MA, USA), The secondary antibodies, conjugated with either carbocyanine 3 (Cy3) or fluorescein isothiocyanate (FITC), were purchased from Jackson ImmunoResearch Laboratories, Inc. (West Grove, PA, USA).

Electronic microscopy

For transmission electron microscopy (TEM), 2% PFA /2% glutaraldehyde-fixed eyes were dissected to remove the cornea and lens, and then post-fixed in 2% osmium tetroxide in phosphate buffer. Retinal tissue was dehydrated in a series of ascending ethanol concentrations (10%, 25%, 50%, 70%, 95% at 10 minutes per concentration, and 100% for 1 hour) and embedded. Blocks of retinal tissue were cut into sections using a Leica EMUC6 Ultramicrotome (Leica Microsystems, Buffalo Grove, IL, USA) prepared as previously described (30, 31), and examined with a transmission electron microscope (TEM; Model 300: Phillips, Eindhoven, Netherlands). Photomicrographs were captured with a digital camera (15 mega pixel digital camera, Scientific Instruments and Applications, Duluth, GA, USA) and Maxim DL Version 5 software (Diffraction Limited, Ottawa, Canada).

Preparation of tissue whole mounts and whole mount immunostaining

In order to simultaneously view all the cells within the RPE layer, epithelial flat-mounts were prepared. Briefly, enucleated eyes were fixed in 4% PFA for overnight at 4°C. After several rinses in PBS, eyecups were prepared by making a circumferential incision at posterior to the ora serrata, and the anterior segments, i.e., cornea, ciliary body, and lens, were discarded. The neural retina was subsequently peeled away from these eyecups, resulting in an intact epithelium partitioning with the choroid, to which it is adherent. The resulting RPE-choroid-sclera whole-mounts were labeled using primary antibodies followed by fluorescent-dye conjugated secondary antibodies. After several tris-buffered saline (TBS) rinses, flat-mounts were placed on glass slides with the epithelium facing up and mounted in

Vectashield fluorescence mounting medium (Vector Labs, Burlingame, CA, USA),and examined using a Zeiss Axio Imayger M2 system equipped with ApoTome, AxioCam and AxioVision (Zeiss, Peabody, MA, USA). In certain cases, nuclear staining was additionally carried out by exposure to propidium iodide (0.1 mg/ml in TBS, containing 0.5 mg/ml RNAase A; Roche, Basel, Switzerland). To ensure that the retina laid flat, several radial cuts (5–6, depending on the size of the eye) were made in the tissue from the periphery to the optic nerve area,

RPE sheets collection

We adapted and modified a previously published procedure for harvesting the entire RPE tissue as a single intact sheet (26). Briefly, the enucleated eyes were collected and washed several time in PBS, then dipped into an Eppendorf tube containing PBS/penicillin-streptomycin medium and 10% Dispase II (Roche, Basel, Switzerland) at 4 °C. After overnight incubation (12–16 hrs), the eye balls were rinsed for a few times with PBS/penicillin-streptomycin, then transferred to a new petri dish containing PBS under a dissecting microscopy. The cornea, iris epithelium, lens and neural retina were gently removed and discarded, then the RPE sheet was peeled off from the choroid using a pair of tweezers. The RPE sheets were transferred to a new Eppendorf tube and spun at 1000 rpm for 5 min. The supernatant was discarded and the RPE sheet pellets were further lysed for protein or RNA isolation. Each RNA and protein sample was extracted from pooled RPE sheets of 5 mice.

Subretinal injection of adeno-associated virus type 2 (AAV2)

The AAV2 vector carried a Cre recombinase expression cassette driven by a RPE-specific RPE65 promoter was purchased from Vector Biosystems Inc. (Malvern, PA, USA). 2.59×10^9 AAV genome copies in 1 μl PBS were delivered by subretinal injection into *Yap1*$^{fl/fl}$/*GFP*$^{+}$ or control *GFP*$^{+}$ mice at 5 weeks of age. Mouse pupils were dilated with a single drop mixture of tropicamide and phenylephrine hydrochloride. Two minutes later, the mice were injected with Ketamine- Xylazine solution. Mice were kept on a 37 °C pad after anesthetic injection and surgery. The cornea was topically anesthetized with one drop of proparicaine. The mouse usually achieves adequate anesthesia within approximately 5 min. The mouse eye was grasped with curved forceps held in the surgeon's left hand so that the eye will be slightly proptosed from pinching of the forceps. The mouse eye was decompressed with 33G needle tip by inserting the needle through the conjunctiva and sclera at 1 mm behind the limbus under an ophthalmic microscope. The beveled needle was removed and replaced with a blunt 35-gauge needle that was attached to Microinjector UMP3 (Word precision instruments, Sarasota, FL, USA). The tip of the blunt needle was inserted between the sclera and retina and advanced to the center. Eight days after injection, RPE flat mount sheets were collected and examined for immunohistochemical analysis.

RNA isolation, quantitative (q) PCR, and Western blot analysis

The experimental methods were previously described (32). The primers for mouse *Yap1* (ID: 15928514a1), mouse Rgr (ID: 10946656a1), mouse *Rdh5* (ID: 19549323a1), mouse *Rpe65* (ID: 19920338a1), and mouse *Ribp1* (ID: 10181110a1), *ctnnb1* (ID: 6671684a1), *Tcf7* (ID: 6678245a1), *Cdh2* (ID: 6680902a1), *Twist1* (ID: 6755907a1), and *Twist2* (ID: 6681177a1)

were designed based on the online PrimerBank database (Harvard Medical School, Boston, MA; http://pga.mgh.harvard.edu/primerbank). *Actin*, *Zeb1*, and *Zeb2* primers were previously reported (32, 33). The antibodies used for Western blot analysis include mouse anti-YAP1 antibody (1:100, cat. # sc-101199, Santa Cruz Biotechnology, Santa Cruz, California, USA), mouse anti-β-actin antibody (1:1000, cat. # A2228, MilliporeSigma, Burlingto, MA, USA), mouse anti-α-tubulin antibody (1:500, cat. # T9026, MilliporeSigma, Burlingto, MA, USA), mouse anti pY654-β-catenin (1:20, cat. # PY654-B-catenin (IgG)-s, DSHB, Iowa City, IA, USA), rabbit anti-β-catenin (D10A8) (1:100, cat. # 8480S, Cell Signaling Technology, Danvers, MA, USA), and mouse anti RPE65 (1:100, cat. # MB5428, MilliporeSigma, Burlingto, MA, USA).

Statistical analysis

Data are reported as the mean±SEM, using multiple mice (3–14) for any quantitative assay. Statistical comparisons between experimental groups were conducted using Student's t-test.

Results

Best1-Cre leads to mosaic pattern of *Yap1* gene deletion in adult RPE *in vivo*

Anti-YAP1 immunohistochemistry showed that YAP1 mainly localizes in the cytoplasm of adult RPE cells (Fig. 1A). Localization of YAP1 to the cytoplasm allowed us to explore the role of YAP1 in differentiated RPE. We generated a conditional knockout mouse line in which the loxP floxed *Yap1* gene was deleted by Best1 promoter-driven Cre recombinase (Best1-Cre). To confirm RPE –specific expression of Best1-Cre, we utilized the *mT/mG* (membrane-Tomato/membrane-Green) dual color fluorescent Cre-reporter transgenic mice which specifically expressed GFP in the Cre expressing cells (28). Consistent with the previous report (27), cell membrane-targeted GFP expression was restricted to RPE cells in *Best1-Cre*$^{+}$*/GFP*$^{+}$ mice Fig. 1B–D). Our *Best1-Yap1-GFP* conditional knockout (cKO) line was generated by crossing *Best1-cre/GFP* mice with *Yap1*$^{fl/fl}$ mice, and then interbreeding further generated the *Best1-Cre*$^{+}$*/Yap1*$^{fl/fl}$*/GFP*$^{+}$ cKO mice and *Best1-Cre*$^{+}$*/GFP*$^{+}$ control mice. Anti-YAP1 immunostaining on whole mount RPE confirmed the loss of YAP1 expression in the GFP positive RPE cells, but remained relatively unchanged in neighboring GFP negative RPE cells in *Best1-Cre*$^{+}$*/GFP*$^{+}$*/Yap1*$^{fl/fl}$ mice (Fig. 1E). This mosaic YAP1 knockout pattern was consistent with previous report that Best1 promoter was specifically active in postnatal RPE cells, but with a patchy mosaic expression pattern of 50% to 90% RPE cells expressing *Cre* (27). YAP1 expression was unaffected in GFP positive RPE cells of *Best1-Cre*$^{+}$*/GFP*$^{+}$ control mice, and the unaffected cells were indistinguishable from GFP negative RPE cells (data not shown). Consistently, further fluorescence immunostaining on retina sections from *Best1-Cre*$^{+}$*/GFP*$^{+}$*/Yap1*$^{fl/fl}$ mice showed that YAP1 protein was present in WT (GFP negative) RPE cells, but not in *Yap1* deleting (GFP positive) RPE (Fig. 1F).

YAP1 is required for maintenance of RPE differentiation

To analyze RPE phenotype, we first examined mice at 1 −2 months of age with fundoscopy prior to enucleation. Retinal fundoscopic photographs showed extensive abnormal depigmentation of the retina in cKO mice (Fig. 2B vs. 2A), indicative of RPE abnormalities. To further analyze retinal phenotype, we evaluated sheets of RPE flat mounts and found that

depigmented patches correlated with *Yap1* mutant (GFP positive) RPE cells in the mutant mice (Fig. 2C). RPE morphology was revealed by actin cytoskeleton labelled with rhodamine-phalloidin on flat mount RPE sheets, and demonstrated a typical hexagonal array of RPE cells in WT control mice with a sharp F-actin network at cell boundaries (Fig. 2C left). Whereas, *Yap1* mutants displayed disorganized RPE cells with irregular shape, increased cell surface area, and a disrupted F-actin network at *Yap1* mutant (GFP-positive) cell boundaries (Fig. 2C right). Mutant RPE cells had an increased surface area (2.8-fold) compared with wild type RPE cells (Fig. 2D). It was notable that GFP and Cre expression per se in RPE did not affect RPE morphology in *Best1-Cre*$^{+}$*/GFP*$^{+}$ control mice (Fig. 2C left). Semi-thin sections (1-μm) showed significantly flattened mutant RPE with loss of pigment granules, suggesting that enlarged surface areas in mutant RPE might be caused by cell flattening without increasing cell volume (Fig. 2E vs 2F, 2G). Transmission electron microscopy on the sections of adult WT and cKO mouse retina from 2 months old animals further revealed a substantial decrease in RPE thickness, retraction of apical microvilli, and basal membrane infoldings, indicative of the loss of normal RPE morphology (Fig. 2H vs 2I). We further quantified the changes on ultrastructural changes using EM images. Number of electron-dense pigment granules in the mutant RPE was significantly reduced with 92% decrease relative to the wild-type Fig. 2J). Retraction of apical microvilli and basal membrane infoldings in the mutant RPE resulted in 51 and 68% shrinkage of paracellular space occupied by apical microvilli and basal unfolding, respectively (Fig. 2J).

Loss of RPE-characteristic marker RPE65 in *Yap1*$^{-/-}$ RPE cells

RPE65 is a key differentiation marker for RPE, and a critical retinol isomerase for isomerization of all-trans-retinal to 11-cis-retinol in phototransduction (34). Loss of RPE65 expression in *Yap1* mutant (GFP positive) RPE cells was a dominant phenotype of the *Best1-Cre*$^{+}$*/GFP*$^{+}$*/Yap1*$^{fl/fl}$ mice Fig. 3B-c, -d, versus WT in Fig. 3A-b). RPE are highly polarized epithelial cells with specialized microvilli at the apical surface intermingled with outer segments of photoreceptors. Notably, GFP used in the *Best1-Cre* mice had a cell membrane targeting sequence, and GFP expression on the cell membrane highlighted the microvilli extension pattern in *Best1-Cre*$^{+}$*/GFP*$^{+}$ WT RPE Fig. 3A-a) and abnormal microvilli retraction in the *Yap1* mutant RPE Fig. 3B-a). This difference in microvilli was further confirmed by Ezrin immunostaining Fig. 3A-c vs 3B-e, -f). Ezrin is specifically associated with apical microvilli of RPE and its staining revealed the difference in the length of RPE microvilli between WT and mutant RPE. This data indicates that *Yap1* mutant RPE cells underwent dramatic dedifferentiation highlighted by cell depolarization and loss of the RPE differentiation marker RPE65, which represent the classic features of epithelial-mesenchymal transition (EMT) often seen in the epithelium during wound healing, in carcinoma, and in RPE during proliferative vitreoretinopathy (PVR). We performed q-PCR mRNA quantification on the RNA samples isolated from RPE sheets of WT or *Best1-cre*$^{+}$*/Yap1*$^{fl/fl}$ eyes to further confirm dedifferentiation. Due to mosaic expression of Best1-Cre, approximately 70% of RPE had homologous recombination and 30% of RPE were genetically WT in the mutant RPE sheets, as judged by fundoscopy. Accordingly, *Yap1* in *Best1-Cre*$^{+}$*/GFP*$^{+}$*/Yap1*$^{fl/fl}$ RPE sheets was reduced to 33% of that in WT controls. Expression of the visual cycle genes *Rgr, Rdh5, Rpe65, and Rlbp1* was also significantly reduced compared to WT littermates (Fig. 3C).

Loss of YAP1 leads to dedifferentiation of RPE cells in adult mice

RPE65 expression is developmentally regulated (35) and RPE65 mRNA is detectable as early as embryonic day 18. Its expression level peaked twice during rat retinal development between P2-P4 and P10-P12 (36). Best1-Cre was reported to appear at P10, reached a peak at p28, and remained constant thereafter (27). To further confirm that loss of RPE 65 expression in *Best-cre*$^{+}$*/Yap1*$^{fl/fl}$ mutant mice was not due to a developmental defect on RPE65 expression but rather dedifferentiation characterized by loss of RPE65 expression, we studied the consequences of targeted knockout of *Yap1* in adult mouse RPE using AAV-mediated Cre gene transfer into *Yap1*-floxed RPE cells. AAV vectors that encode *Cre* under control of a RPE65 promoter were packaged in an AAV2 capsid. 5×10^{10} AAV genome copies in 1 μl were delivered by subretinal injection into *Yap1*$^{fl/fl}$*/GFP*$^{+}$ or control *GFP*$^{+}$ mice at 5 weeks of age. 8 days after injection, RPE flat mounts were examined for morphological abnormalities. We detected about 60% of RPE cells were targeted by AAV2-RPE65-Cre in both wild type and mutant mice as visualized by GFP expression which is turned on in the cells transduced by AAV2-RPE65-Cre Fig. 4A–B first rows). Similar to *Best1-cre*$^{+}$*/Yap1*$^{fl/fl}$ genetic mice, *Yap1* mutant RPE (GFP positive) cells appear enlarged with less stain by rhodamine-phalloidin (Fig. 4B) compared to adjacent Yap1 expressing WT RPE (GFP-negative) cells (Fig. 4B) or RPE in control mice (Fig. 4A). *Cre* transduced *Yap1*$^{fl/fl}$*/GFP*$^{+}$ RPE cells showed lost immunostaining for RPE65 in the flat mount RPE sheet (Fig. 4C) or retina section (Fig. 4D). Our results indicate that the loss of mature RPE morphology seen in the *Yap1* cKO mice is caused by loss of YAP1- induced dedifferentiation, and not by inhibition of initial RPE differentiation during the early development.

EMT-like phenotypic changes of *Yap1* mutant RPE

We showed that *Yap1* mutation in mice after RPE differentiation led to diminished tight junctions, loss of RPE65 and pigment, and retraction of microvilli and basal infoldings. These are classic features of EMT, which are also evident in RPE during PVR. To explore the molecular pathways involved in the EMT-like phenotype of *Yap1* mutant RPE, we examined the activity of Wnt/β-catenin pathway that is considered an important regulator of epithelial stability and EMT. Activation of Wnt/β-catenin pathway induces cytosolic accumulation of β-catenin and then nuclear translocation for activation of gene targets involved in EMT. B-catenin was expressed on the RPE cell membranes in RPE cell of *Best1-Cre*$^{+}$*/GFP*$^{+}$ control mice (Fig. 5A, left) and wild type RPE cells (GFP negative cells in Fig. 5A, right) in *Yap1* cKO mice without clear nuclear localization. However, a diffuse intracellular accumulation of β-catenin was clearly detected in *Yap1* deleting (GFP positive) RPE (Fig. 5A, right). Meanwhile, cytoplasmic β-catenin was restricted to very low levels in either GFP-positive or GFP-negative WT RPE cells in the control mice, eliminating Cre or GFP as a phenotype-causing factor (Fig. 5A, left). Consistently, immunostaning of YAP1 on RPE flatmounts showed that β-catenin dissociated from cell membrane and moved into the nuclei of *Yap1* mutant RPE (labeled by GFP^{+} in the right panels) (Fig. 5B). We next examined phosphorylation of β-catenin Tyr654, which is known to promote both dissociation of β-catenin from E-cadherin and promote EMT (37–39). We isolated protein from RPE sheets. Western blot analysis on RPE lysates showed that the YAP1 protein level in the mutant RPE sheets was reduced to about 27% of that in the WT RPE sheets,

suggesting that about 73% of RPE cells from the mutant mice underwent *Yap1* gene deletion. Consistently, RPE65 protein levels in the mutant RPE sheets was reduced to about 26% of that in the WT RPE sheets. There was a mild 1.5-fold increase in total β-catenin protein and a significant 3.4-fold increase in pY654 β-catenin in the mutant RPE sheets compared to the WT RPE sheets (Fig. 5C). The β-catenin mRNA level was not changed in the mutant RPE cells and transcription of *Tcf7*, a transcriptional target of Wnt/β-catenin pathway, was significantly induced in *Yap1* mutant RPE (Fig. 5D). EMT is usually associated with upregulation of EMT markers, such as *Cdh2*, *Zeb1*, *Zeb2*, *Twist1*, and *Twist2*. We noted an increase in *Chd2* and *Zeb1* expression, but no significant changes in the other examined factors including *Zeb2* and *Twist1* and *Twist2*, suggesting an unique molecule characteristics of *Yap1* mutant RPE (Fig. 5D). These data suggest that Wnt/β-catenin pathway is activated in *Yap1* mutant RPE.

Progressive loss of photoreceptors and ERG response in *Best1-Cre*$^{+}$*/GFP*$^{+}$*/Yap1*$^{fl/fl}$ mice

RPE plays several critical roles in maintaining photoreceptor function. Histology showed that *Yap1* cKO RPE led to photoreceptor degeneration and reduced thickness in the photoreceptor outer nuclear layer over time (Fig. 6A). Depletion of *Yap1* in ≥ 80% of adult RPE led to photoreceptor degeneration in 50% of the mutant mice by 6 months of age (n=14 mice), and the photoreceptor outer nuclear layer was completely lost in some of the mutant mice Fig. 6B–C). Consequently, electroretinography was also significantly affected Fig. 6D–E). At 2 months of age, the ERG was normal in the mutant mice (data not shown); however, there was a significant reduction of scotopic a-wave and b-wave amplitudes by 4–6 months of age Fig. 6D–E). These results suggest that loss of YAP1 in RPE cells can cause photoreceptor degeneration and visual loss.

Discussion

Mounting evidence suggests that cell differentiation is not irreversible process, and maintenance of a mature cell type at its fully differentiated statues requires coordinating regulations of a complicate molecular network. Loss of a normal differentiation phenotype is frequently detrimental, as in the cases of cancer and metastatic diseases. Understanding of mechanisms underlying intracellular signaling pathways and transcriptional regulation for cell fate decisions, maintenance of cellular identities *in vivo* become eminent. Recent work performed on the zebrafish embryonic RPE has demonstrated an essential role of YAP1 in RPE cell fate determination (21). YAP1-dependent RPE fate determination relies on both nuclear localization of YAP1 and interaction with TEAD transcription factors (21). Our study using conditional gene ablation in mice further demonstrated YAP1 was constantly required to prevent dedifferentiation of the adult RPE cells. We observed that the loss of Yap1 in RPE led to changes of cell morphology, loss of molecular signature RPE65 gene and other important visual cycle genes. It was noteworthy that Wnt/β-catenin activity was clearly induced in the cells without YAP1.

YAP1 is a major down-stream factor that regulates cell proliferation and tissue size in response to various cellular signals (40). The central dogma is that YAP1 localization is dynamically controlled during epithelial cell development, i.e., nuclear Yap1 is required for

progenitor proliferation and expansion, and a subsequent shift of Yap1 from the nucleus to the cytoplasm is associated with cell differentiation, as demonstrated in the epithelia of the epidermis (32, 41, 42), lung (43, 44), liver and intestine (45). YAP1 activation leads to cell proliferation in multiple tissues and promotes multiple human cancers through interacting with TEAD family transcription factors. In contrast to the classical role of Yap1 as a cell proliferation regulator, in the present study, we showed that Yap1 was essential for maintaining adult RPE differentiation and loss of Yap1 altered cell fate and function leading to photoreceptor loss and visual impairment. We injected WT and *Yap1* knockout mice with BrdU to follow cell proliferation. As expected, we failed to detect proliferation of the RPE in WT mice, and neither WT nor mutant RPE were proliferating in *Yap1* knockout littermates (data not shown).

In the present study, we showed that deleting Yap1 induced Wnt/β-catenin activity and caused RPE dedifferentiation. Although Wnt/β-catenin is required for RPE morphogenesis in embryos (46, 47), re-activation of this signaling pathway in adult RPE is known to cause EMT and loss of RPE identity (48–51). This is consistent with the functional role of the Wnt/β-catenin pathway in dedifferentiation of epithelial phenotype and induction of EMT, as well as in embryogenesis and cancer progression. Although YAP1 regulation of β-catenin stability in RPE is not clear, studies in TAZ, an ortholog of YAP1, suggest that cytoplasmic TAZ/YAP1 blocks DVL phosphorylation, an event required for β-catenin release from a degradation complex leading to enhanced cytoplasmic expression of β-catenin (52). Similarly, YAP1 has been shown to inhibit Wnt/β-catenin signaling by binding to DVL in intestinal epithelium (53). Our studied showed a similar repressing effect of YAP1 on Wnt/β-catenin activity. YAP1 was mainly localized in the cytoplasm of adult mouse RPE cells as detected by immunostaining. Loss of YAP1 from adult RPE resulted in the change of β-catenin localization, i.e. from membrane bound to a diffused intracellular expression pattern. The induced β-catenin phosphorylation at Tyr-654 was regarded as a critical determinant of EMT in pulmonary fibrosis (39), and pY-654-β-catenin was significantly accumulated without change of β-catenin mRNA level. β-catenin nuclear transcription activity was enhanced as evidenced by increased transcription of the β-catenin target genes. From those observations, we hypothesize that cytoplasmic YAP1 in adult RPE cells may primarily act to inhibit β-catenin activity to maintain the RPE at differentiation status, albeit this hypothesis needs to be further addressed.

Although the molecular details underlying YAP1 function in adult RPE remain to be clarified, its functional significance in maintenance of RPE at differentiation has been demonstrated in the present work. Maintenance of RPE at a differentiation state is essential for photoreceptor survival and function, and visual activity. Dysfunctional RPE is a key pathologic hallmark observed in many different retinal diseases, such as age-related macular degeneration, a leading cause of blindness in the U.S (54), and inherited retinal dystrophies. Differentiation of hESCs toward a RPE fate is an active area being explored for the treatment of many retinal dystrophies. Elucidating Yap1 function in maintaining the adult RPE cell fate and RPE65 expression will be important in stem cell and RPE therapy (52–54). Our cKO model may serve as an appropriate mouse model for studying the molecular mechanisms controlling mature RPE identity, polarity, and function. It may also serve as a suitable model for studying RPE EMT and its role in other retinal diseases.

Acknowledgements

This research was supported by NIH grants EY027033. This work was also supported in part by an unrestricted institutional grant from Research to Prevent Blindness, NY.

Abbreviations:

RPE	retinal pigment epithelium
DVL	disheveled
cKO	conditional knockout
AAV	Adeno-associated virus
EMT	epithelial-mesenchymal transition
PCR	proliferative vitreoretinopathy
TEM	transmission electron microscopy
PFA	paraformaldehyde
fl	floxed
WT	wild type
MUT	mutant
GFP	green fluorescent protein
ERG	electroretinography
HE	hematoxylin and eosin

References

1. Dong J, Feldmann G, Huang J, Wu S, Zhang N, Comerford SA, Gayyed MF, Anders RA, Maitra A, and Pan D (2007) Elucidation of a universal size-control mechanism in Drosophila and mammals. Cell 130, 1120–1133 [PubMed: 17889654]
2. Piccolo S, Dupont S, and Cordenonsi M (2014) The biology of YAP/TAZ: hippo signaling and beyond. Physiological reviews 94, 1287–1312 [PubMed: 25287865]
3. Yu FX, and Guan KL (2013) The Hippo pathway: regulators and regulations. Genes & development 27, 355–371 [PubMed: 23431053]
4. Zhao B, Li L, Lei Q, and Guan KL (2010) The Hippo-YAP pathway in organ size control and tumorigenesis: an updated version. Genes & development 24, 862–874 [PubMed: 20439427]
5. Kodaka M, and Hata Y (2015) The mammalian Hippo pathway: regulation and function of YAP1 and TAZ. Cellular and molecular life sciences : CMLS 72, 285–306 [PubMed: 25266986]
6. Pan D (2010) The hippo signaling pathway in development and cancer. Developmental cell 19, 491–505 [PubMed: 20951342]
7. Barry ER, and Camargo FD (2013) The Hippo superhighway: signaling crossroads converging on the Hippo/Yap pathway in stem cells and development. Curr Opin Cell Biol 25, 247–253 [PubMed: 23312716]

8. Schlegelmilch K, Mohseni M, Kirak O, Pruszak J, Rodriguez JR, Zhou D, Kreger BT, Vasioukhin V, Avruch J, Brummelkamp TR, and Camargo FD (2011) Yap1 acts downstream of alpha-catenin to control epidermal proliferation. Cell 144, 782–795 [PubMed: 21376238]

9. Silvis MR, Kreger BT, Lien WH, Klezovitch O, Rudakova GM, Camargo FD, Lantz DM, Seykora JT, and Vasioukhin V (2011) alpha-catenin is a tumor suppressor that controls cell accumulation by regulating the localization and activity of the transcriptional coactivator Yap1. Sci Signal 4, ra33 [PubMed: 21610251]

10. Azzolin L, Panciera T, Soligo S, Enzo E, Bicciato S, Dupont S, Bresolin S, Frasson C, Basso G, Guzzardo V, Fassina A, Cordenonsi M, and Piccolo S (2014) YAP/TAZ incorporation in the beta-catenin destruction complex orchestrates the Wnt response. Cell 158, 157–170 [PubMed: 24976009]

11. Robinson BS, and Moberg KH (2011) Cell-cell junctions: alpha-catenin and E-cadherin help fence in Yap1. Curr Biol 21, R890–892 [PubMed: 22075429]

12. Chan SW, Lim CJ, Chong YF, Pobbati AV, Huang C, and Hong W (2011) Hippo pathway-independent restriction of TAZ and YAP by angiomotin. J Biol Chem 286, 7018–7026 [PubMed: 21224387]

13. Wang W, Huang J, and Chen J (2011) Angiomotin-like proteins associate with and negatively regulate YAP1. J Biol Chem 286, 4364–4370 [PubMed: 21187284]

14. Zhao B, Li L, Lu Q, Wang LH, Liu CY, Lei Q, and Guan KL (2011) Angiomotin is a novel Hippo pathway component that inhibits YAP oncoprotein. Genes & development 25, 51–63 [PubMed: 21205866]

15. Zhao B, Wei X, Li W, Udan RS, Yang Q, Kim J, Xie J, Ikenoue T, Yu J, Li L, Zheng P, Ye K, Chinnaiyan A, Halder G, Lai ZC, and Guan KL (2007) Inactivation of YAP oncoprotein by the Hippo pathway is involved in cell contact inhibition and tissue growth control. Genes & development 21, 2747–2761 [PubMed: 17974916]

16. Zhao B, Li L, and Guan KL (2010) Hippo signaling at a glance. J Cell Sci 123, 4001–4006 [PubMed: 21084559]

17. Zhao B, Tumaneng K, and Guan KL (2011) The Hippo pathway in organ size control, tissue regeneration and stem cell self-renewal. Nat Cell Biol 13, 877–883 [PubMed: 21808241]

18. Lee Y, Kim NH, Cho ES, Yang JH, Cha YH, Kang HE, Yun JS, Cho SB, Lee SH, Paclikova P, Radaszkiewicz TW, Bryja V, Kang CG, Yuk YS, Cha SY, Kim SY, Kim HS, and Yook JI (2018) Dishevelled has a YAP nuclear export function in a tumor suppressor context-dependent manner. Nat Commun 9, 2301 [PubMed: 29895829]

19. Strauss O (2005) The retinal pigment epithelium in visual function. Physiological reviews 85, 845–881 [PubMed: 15987797]

20. Asaoka Y, Hata S, Namae M, Furutani-Seiki M, and Nishina H (2014) The Hippo pathway controls a switch between retinal progenitor cell proliferation and photoreceptor cell differentiation in zebrafish. PloS one 9, e97365 [PubMed: 24828882]

21. Miesfeld JB, Gestri G, Clark BS, Flinn MA, Poole RJ, Bader JR, Besharse JC, Wilson SW, and Link BA (2015) Yap and Taz regulate retinal pigment epithelial cell fate. Development 142, 3021–3032 [PubMed: 26209646]

22. Jiang Q, Liu D, Gong Y, Wang Y, Sun S, Gui Y, and Song H (2009) yap is required for the development of brain, eyes, and neural crest in zebrafish. Biochemical and biophysical research communications 384, 114–119 [PubMed: 19393221]

23. Cabochette P, Vega-Lopez G, Bitard J, Parain K, Chemouny R, Masson C, Borday C, Hedderich M, Henningfeld KA, Locker M, Bronchain O, and Perron M (2015) YAP controls retinal stem cell DNA replication timing and genomic stability. Elife 4, e08488 [PubMed: 26393999]

24. Kim JY, Park R, Lee JH, Shin J, Nickas J, Kim S, and Cho SH (2016) Yap is essential for retinal progenitor cell cycle progression and RPE cell fate acquisition in the developing mouse eye. Developmental biology 419, 336–347 [PubMed: 27616714]

25. Yoshida K, Nakayama K, Kase S, Nagahama H, Harada T, Ikeda H, Harada C, Imaki J, Ohgami K, Shiratori K, Ohno S, Nishi S, and Nakayama KI (2004) Involvement of p27(KIP1) in proliferation of the retinal pigment epithelium and ciliary body. Anat Embryol (Berl) 208, 145–150 [PubMed: 15007644]

26. Defoe DM, Adams LB, Sun J, Wisecarver SN, and Levine EM (2007) Defects in retinal pigment epithelium cell proliferation and retinal attachment in mutant mice with p27(Kip1) gene ablation. Molecular vision 13, 273–286 [PubMed: 17356514]
27. Iacovelli J, Zhao C, Wolkow N, Veldman P, Gollomp K, Ojha P, Lukinova N, King A, Feiner L, Esumi N, Zack DJ, Pierce EA, Vollrath D, and Dunaief JL (2011) Generation of Cre transgenic mice with postnatal RPE-specific ocular expression. Investigative ophthalmology & visual science 52, 1378–1383 [PubMed: 21212186]
28. Muzumdar MD, Tasic B, Miyamichi K, Li L, and Luo L (2007) A global double-fluorescent Cre reporter mouse. Genesis 45, 593–605 [PubMed: 17868096]
29. Noel JM, Fernandez de Castro JP, Demarco PJ Jr., Franco LM, Wang W, Vukmanic EV, Peng X, Sandell JH, Scott PA, Kaplan HJ, and McCall MA (2012) Iodoacetic acid, but not sodium iodate, creates an inducible swine model of photoreceptor damage. Experimental eye research 97, 137–147 [PubMed: 22251455]
30. Fernandez de Castro JP, Scott PA, Fransen JW, Demas J, DeMarco PJ, Kaplan HJ, and McCall MA (2014) Cone photoreceptors develop normally in the absence of functional rod photoreceptors in a transgenic swine model of retinitis pigmentosa. Investigative ophthalmology & visual science 55, 2460–2468 [PubMed: 24618325]
31. Scott PA, Fernandez de Castro JP, Kaplan HJ, and McCall MA (2014) A Pro23His mutation alters prenatal rod photoreceptor morphology in a transgenic swine model of retinitis pigmentosa. Investigative ophthalmology & visual science 55, 2452–2459 [PubMed: 24618321]
32. Sambandam SAT, Kasetti RB, Xue L, Dean DC, Lu Q, and Li Q (2015) 14-3-3sigma regulates keratinocyte proliferation and differentiation by modulating Yap1 cellular localization. The Journal of investigative dermatology 135, 1621–1628 [PubMed: 25668240]
33. Liu Y, Ye F, Li Q, Tamiya S, Darling DS, Kaplan HJ, and Dean DC (2009) Zeb1 represses Mitf and regulates pigment synthesis, cell proliferation, and epithelial morphology. Invest Ophthalmol Vis Sci 50, 5080–5088 [PubMed: 19515996]
34. Wolf G (2005) Function of the protein RPE65 in the visual cycle. Nutr Rev 63, 97–100 [PubMed: 15825812]
35. Hamel CP, Tsilou E, Harris E, Pfeffer BA, Hooks JJ, Detrick B, and Redmond TM (1993) A developmentally regulated microsomal protein specific for the pigment epithelium of the vertebrate retina. J Neurosci Res 34, 414–425 [PubMed: 8474143]
36. Manes G, Leducq R, Kucharczak J, Pages A, Schmitt-Bernard CF, and Hamel CP (1998) Rat messenger RNA for the retinal pigment epithelium-specific protein RPE65 gradually accumulates in two weeks from late embryonic days. FEBS Lett 423, 133–137 [PubMed: 9512345]
37. Murase S, Mosser E, and Schuman EM (2002) Depolarization drives beta-Catenin into neuronal spines promoting changes in synaptic structure and function. Neuron 35, 91–105 [PubMed: 12123611]
38. Roura S, Miravet S, Piedra J, Garcia de Herreros A, and Dunach M (1999) Regulation of E-cadherin/Catenin association by tyrosine phosphorylation. J Biol Chem 274, 36734–36740 [PubMed: 10593980]
39. Ulsamer A, Wei Y, Kim KK, Tan K, Wheeler S, Xi Y, Thies RS, and Chapman HA (2012) Axin pathway activity regulates in vivo pY654-beta-catenin accumulation and pulmonary fibrosis. J Biol Chem 287, 5164–5172 [PubMed: 22203675]
40. Varelas X (2014) The Hippo pathway effectors TAZ and YAP in development, homeostasis and disease. Development 141, 1614–1626 [PubMed: 24715453]
41. Zhang H, Pasolli HA, and Fuchs E (2011) Yes-associated protein (YAP) transcriptional coactivator functions in balancing growth and differentiation in skin. Proc Natl Acad Sci U S A 108, 2270–2275 [PubMed: 21262812]
42. Elbediwy A, Vincent-Mistiaen ZI, Spencer-Dene B, Stone RK, Boeing S, Wculek SK, Cordero J, Tan EH, Ridgway R, Brunton VG, Sahai E, Gerhardt H, Behrens A, Malanchi I, Sansom OJ, and Thompson BJ (2016) Integrin signalling regulates YAP and TAZ to control skin homeostasis. Development 143, 1674–1687 [PubMed: 26989177]

43. Mahoney JE, Mori M, Szymaniak AD, Varelas X, and Cardoso WV (2014) The hippo pathway effector Yap controls patterning and differentiation of airway epithelial progenitors. Developmental cell 30, 137–150 [PubMed: 25043473]
44. Zhao R, Fallon TR, Saladi SV, Pardo-Saganta A, Villoria J, Mou H, Vinarsky V, Gonzalez-Celeiro M, Nunna N, Hariri LP, Camargo F, Ellisen LW, and Rajagopal J (2014) Yap tunes airway epithelial size and architecture by regulating the identity, maintenance, and self-renewal of stem cells. Dev Cell 30, 151–165 [PubMed: 25043474]
45. Mo JS, Park HW, and Guan KL (2014) The Hippo signaling pathway in stem cell biology and cancer. EMBO Rep 15, 642–656 [PubMed: 24825474]
46. Westenskow P, Piccolo S, and Fuhrmann S (2009) Beta-catenin controls differentiation of the retinal pigment epithelium in the mouse optic cup by regulating Mitf and Otx2 expression. Development 136, 2505–2510 [PubMed: 19553286]
47. Fujimura N, Taketo MM, Mori M, Korinek V, and Kozmik Z (2009) Spatial and temporal regulation of Wnt/beta-catenin signaling is essential for development of the retinal pigment epithelium. Developmental biology 334, 31–45 [PubMed: 19596317]
48. Chen HC, Zhu YT, Chen SY, and Tseng SC (2012) Wnt signaling induces epithelial-mesenchymal transition with proliferation in ARPE-19 cells upon loss of contact inhibition. Laboratory investigation; a journal of technical methods and pathology 92, 676–687 [PubMed: 22391957]
49. Umazume K, Tsukahara R, Liu L, Fernandez de Castro JP, McDonald K, Kaplan HJ, and Tamiya S (2014) Role of retinal pigment epithelial cell beta-catenin signaling in experimental proliferative vitreoretinopathy. Am J Pathol 184, 1419–1428 [PubMed: 24656918]
50. Burke JM (2008) Epithelial phenotype and the RPE: is the answer blowing in the Wnt? Progress in retinal and eye research 27, 579–595 [PubMed: 18775790]
51. Tamiya S, Liu L, and Kaplan HJ (2010) Epithelial-mesenchymal transition and proliferation of retinal pigment epithelial cells initiated upon loss of cell-cell contact. Investigative ophthalmology & visual science 51, 2755–2763 [PubMed: 20042656]
52. Buchholz DE, Hikita ST, Rowland TJ, Friedrich AM, Hinman CR, Johnson LV, and Clegg DO (2009) Derivation of functional retinal pigmented epithelium from induced pluripotent stem cells. Stem Cells 27, 2427–2434 [PubMed: 19658190]
53. Idelson M, Alper R, Obolensky A, Ben-Shushan E, Hemo I, Yachimovich-Cohen N, Khaner H, Smith Y, Wiser O, Gropp M, Cohen MA, Even-Ram S, Berman-Zaken Y, Matzrafi L, Rechavi G, Banin E, and Reubinoff B (2009) Directed differentiation of human embryonic stem cells into functional retinal pigment epithelium cells. Cell Stem Cell 5, 396–408 [PubMed: 19796620]
54. Nazari H, Zhang L, Zhu D, Chader GJ, Falabella P, Stefanini F, Rowland T, Clegg DO, Kashani AH, Hinton DR, and Humayun MS (2015) Stem cell based therapies for age-related macular degeneration: The promises and the challenges. Progress in retinal and eye research 48, 1–39 [PubMed: 26113213]

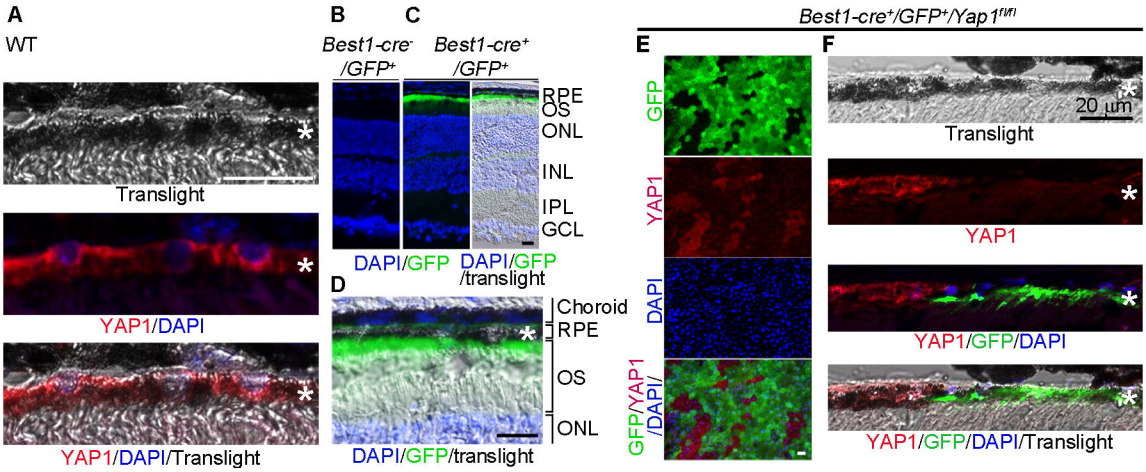

Figure 1.

Mosaic deletion pattern of *Yap1* mediated by Best1-Cre in adult RPE *in vivo*. A, Immunostaining of YAP1 showed cytoplasmic localization in the RPE cells of wild-type mouse at 6-week-old. B,C, *Best1-Cre* was confirmed by GFP expression in the RPE of *Best1-Cre*$^{+}$*/GFP*$^{+}$ (C) but not *Best1-Cre*$^{-}$*/GFP*$^{+}$ mice (B). D, High magnification of image of the right panel in (C). E,F, YAP1 immunostaining showed that YAP1 was only depleted in GFP^{+}, but not in the GFP^{-} RPEs of the *Yap1* cKO mice (*Best1-Cre*$^{+}$*/GFP*$^{+}$*/Yap1*$^{fl/fl}$, MUT). RPE whole mount (E) and RPE tissue section (F) from the *Yap1* cKO mice were immunostained by YAP1 (red), GFP (green), and DAPI (blue). *RPE layer. Bar size = 20 μm. At least 5 animals per group were used for each assay.

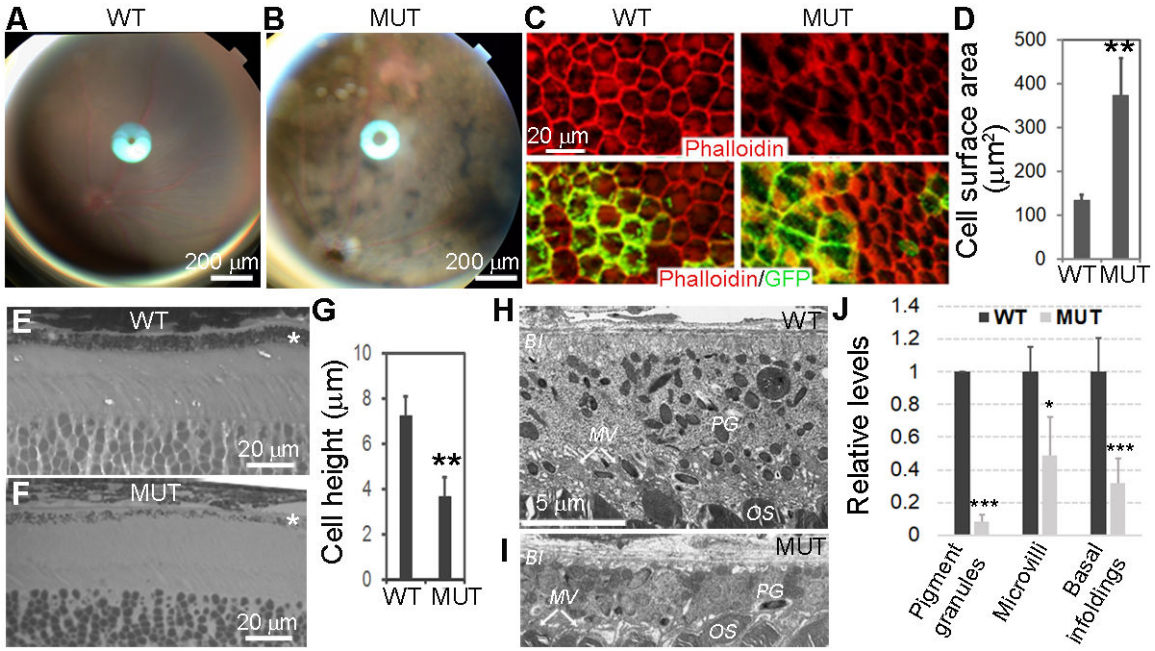

Figure 2.

Morphologic changes of *Yap1*$^{-/-}$ RPE cells. *Yap1* cKO mice (*Best1-Cre*$^{+}$*/GFP*$^{+}$*/Yap1*$^{fl/fl}$, MUT) and control mice (*Best1-Cre*$^{+}$*/GFP*$^{+}$, WT) were analyzed at 5–8 weeks of age. A,B, Fundoscopy of WT (A) and mutant (B) mice, showing uneven mosaic-pattern pigmentation color in mutant. C, Phalloidin (red) and GFP (green) show loss of cuboidal appearance and abnormal cell shape with disrupted F-actin network in the RPE sheets from mutant mice (right panel) compared with WT control mice (left panel). D, The quantitation shows significantly increased cell surface area of *Yap1* mutant RPE cells (green cells in the right panel of C). Value = mean ± SD. n = 3 mice for each group. At least 50 cells were counted per animal. E,F, Methylene blue staining of semi-thin retina sections reveals thinner *Yap1* mutant RPE cells. *RPE layer G) The quantitation shows significantly reduced cell height of *Yap1* mutant RPE cells. Value = mean ± SD. n = 3 mice for each group. At least 10 cells were counted per animal. H-I, Electron microscopy shows normal RPE from WT mice (H) and flattened mutant RPE cells with thinner cell shape and loss of pigment granule (PG), microvilli (MV), and basal infoldings (BI) from the mutant mice (I). OS, photoreceptor outer segment. Images in (H) and (I) are at the same magnification. J, Quantification of pigment granules, microvilli, and basal infoldings in the WT and mutant RPE cells. Number of granules, and area of microvilli and basal infoldings in EM images were quantified by Image J software, then, their relative levels were normalized to RPE cell body area. Their relative comparison between WT and mutant RPE were graphed. Value = mean ± SD. n = 3 mice for each group. At least six cells were counted per animal. *, **, *** are $P < .05$, $P < .01$, $P < .005$, respectively. Bar sizes are indicated on the figures.

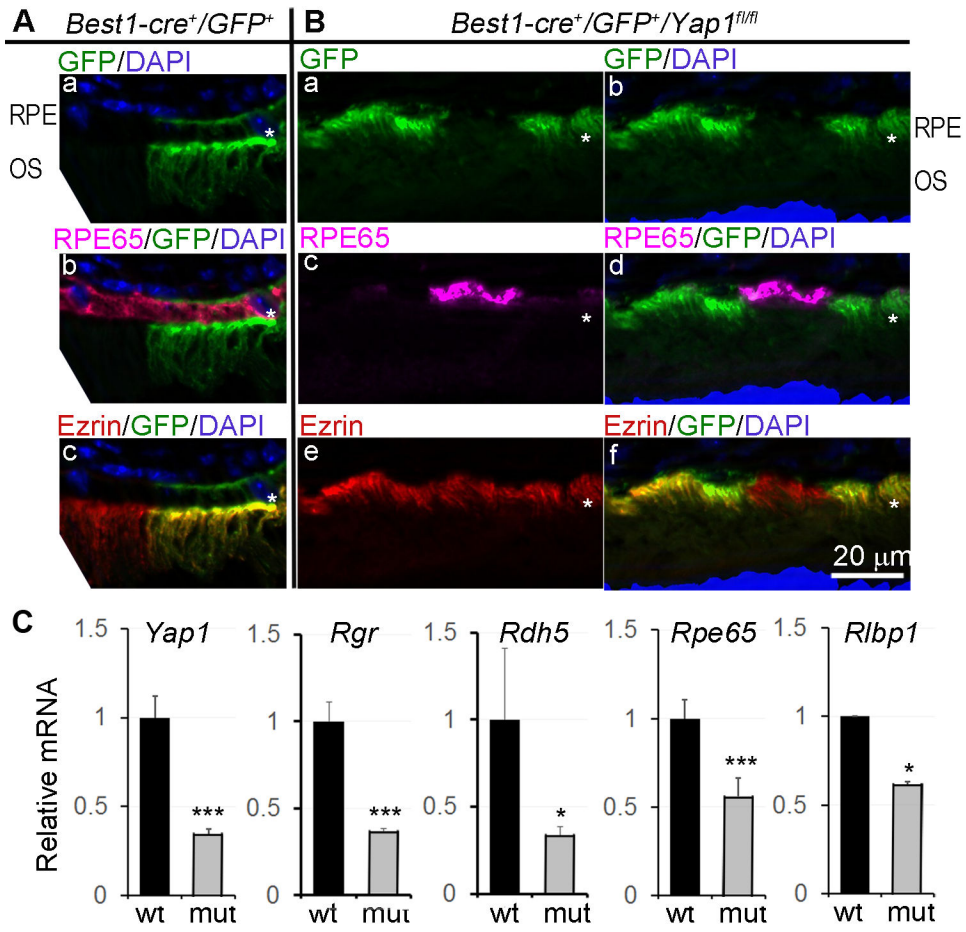

Figure 3.

Loss of RPE65 expression in *Yap1* mutant RPE cells. *Yap1* cKO mice (*Best1-Cre*$^{+}$*/GFP*$^{+}$*/Yap1*$^{fl/fl}$, MUT) and the control mice (*Best1-Cre*$^{+}$*/GFP*$^{+}$, WT) were analyzed at 5–8 weeks of age. A,B, Immunostaining of RPE differentiation markers, RPE65 and Ezrin on the WT (A) and mutant (B) retina sections of 5-week-old mice. * in (A) and (B): RPE layer. Bar size = 20 μm. n = 5 mice for each group. C, qPCR analysis showed reduced expression of RPE65 and other visual cycle genes. Value = mean ± SD. n = 3 samples for each group. Each sample was extracted from pooled RPE sheets of 5 mice. *, *** are P < .05, P < .005, respectively.

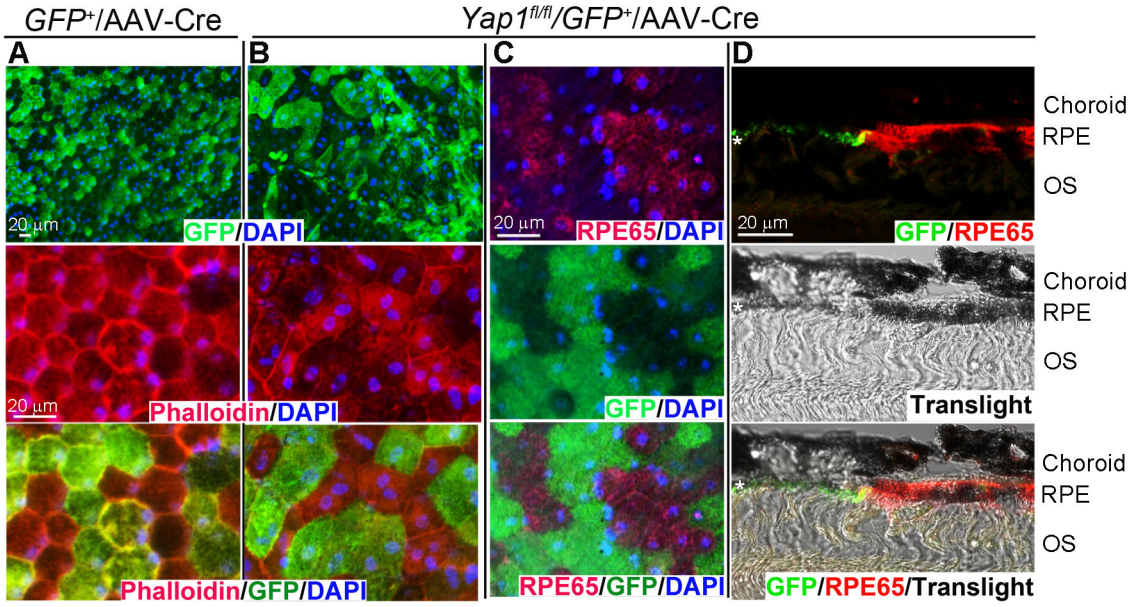

Figure 4.

AAV2-RPE65-Cre mediated *Yap1* deletion leads to RPE dedifferentiation in adult mice. Subretinal injection of 1 μl of AAV2-RPE65-Cre (2.59×10^{12} GC/ml) was performed in *GFP*$^{+}$ (A) and *Yap1*$^{fl/fl}$/*GFP*$^{+}$ (B-D) mice at 5 weeks of age. Eyes were collected at 8 days after subretinal injection. A-B) Whole mount immunostaining of Phalloidin (red), GFP (green), and DAPI (blue) show loss of cuboidal appearance and abnormal cell shape in *Yap1* mutant (GFP positive) cell in (B). C-D) RPE65 expression is lost in *Yap1* mutant (GFP positive) cells mediated by AAV2-RPE65-Cre in whole mount (C) and retina sections (D) by immunostaining. *, RPE layer, n = 3 mice per group for each assay, Bar size = 20 μm.

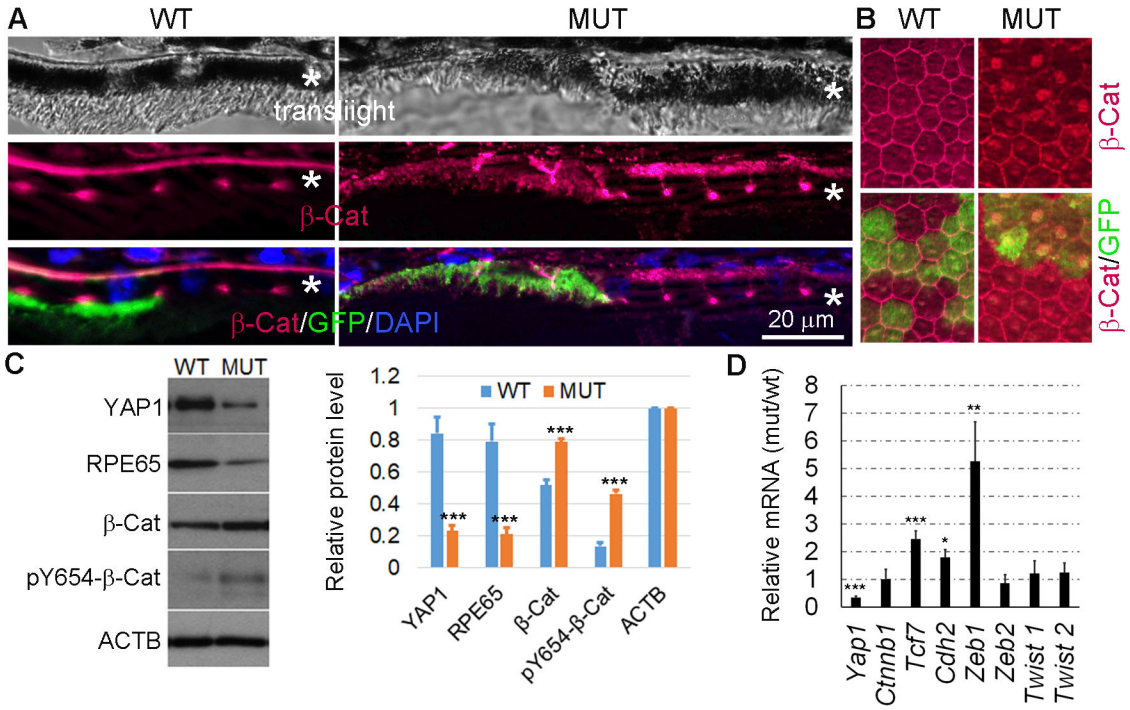

Figure 5.

Increased β-catenin activation in the *Yap1* KO RPE cells. *Yap1* cKO mice (*Best1-Cre*$^{+}$*/GFP*$^{+}$*/Yap1*$^{fl/fl}$, MUT) and the control mice (*Best1-Cre*$^{+}$*/GFP*$^{+}$, WT) were analyzed at 5–8 weeks of age. A, Immunostaining for β-catenin (red) and GFP (green) on the eye tissue section from WT and mutant mice. *RPE layer. n = 3 mice per group for each assay. Bar size = 20 μm. B, Immunostaining for β-catenin (red) and GFP (green) on the RPE whole mount from WT and mutant mice. C, Western blot analysis was performed with protein samples from the RPE sheets collected from WT and mutant mice. The quantification results from Western blot analysis using ImageJ software are shown on the right side, Value = mean ± SD, n = 3 samples per group. Each sample was extracted from pooled RPE sheets of 5 mice. ***P < .005. D, qPCR analysis from the RPE sheets of WT and mutant showed that the β-catenin nuclear target Tcf7 and EMT markers, Cdh2 and Zeb1 are significant increased. Data expressed as mean ± SD, n = 3 samples per group. Each sample were extracted from pooled RPE sheets of 5 mice. *, **, *** are P < .05, P < .01, P < .005.

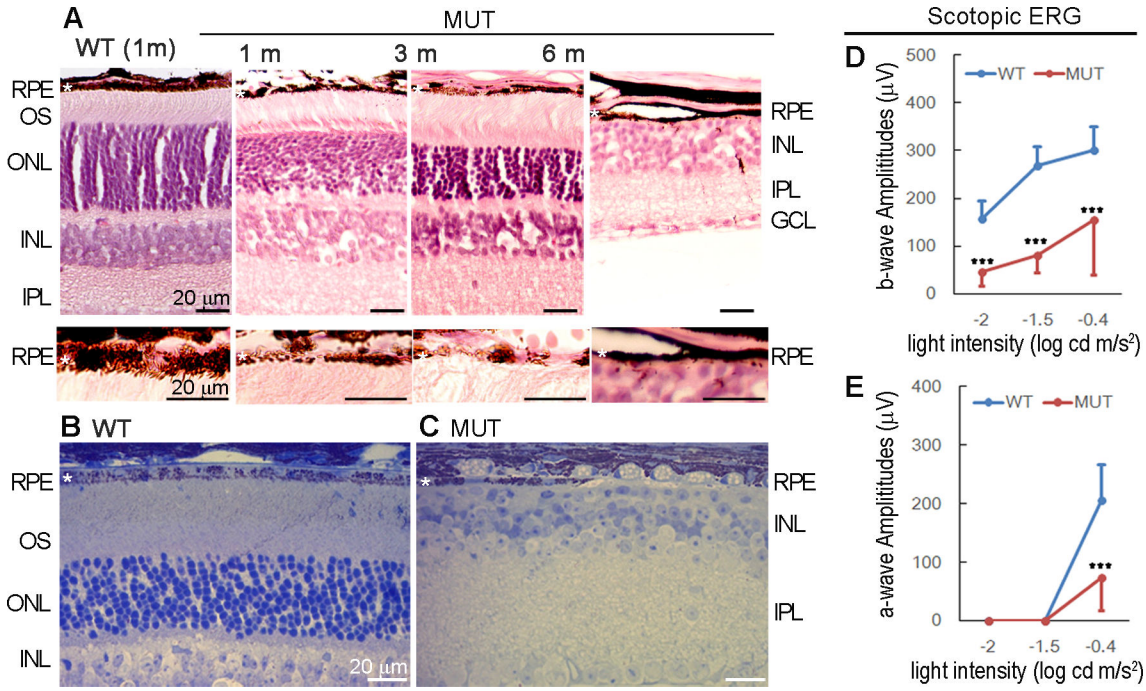

Figure 6.

Progressive loss of photoreceptors and ERG response. *Best1-Cre*$^{+}$*/GFP*$^{+}$*/Yap1*$^{fl/fl}$ (MUT) mutant mice and *Best1-Cre*$^{+}$*/GFP*$^{+}$ (WT) control nice were analyzed. A) HE staining of eye tissue sections from WT and mutant mice at the indicated ages. B-C) Methylene blue staining of semi-thin retinal sections of 6 months old of WT and mutant mice. D-E) Full field ERG analysis showed scotopic b-wave (D) and a-wave (E) values of WT (blue) and mutant (red) mice at 4–6 months. Value = mean±SD, n = 6 mice per group ***, $p < 0.005$.